The Journal of the Acoustical Society of America

# A quasi-uniform acoustic leaky-wave antenna: Analysis, design and experimental validation

--Manuscript Draft--

| | |
|---|---|
| **Manuscript Number:** | |
| **Full Title:** | A quasi-uniform acoustic leaky-wave antenna: Analysis, design and experimental validation |
| **Article Type:** | Regular Article |
| **Corresponding Author:** | Jens Forssén, PhD<br>Chalmers University of Technology: Chalmers tekniska hogskola AB<br>SWEDEN |
| **First Author:** | Jens Forssén, PhD |
| **Order of Authors:** | Jens Forssén, PhD |
| | Pablo-Antonio Martínez-Vicente |
| | Astrid Algaba-Brazález |
| | Matthew Polidano |
| | José-Luis Gómez-Tornero |
| **Section/Category:** | Physical Acoustics |
| **Keywords:** | acoustic leaky-wave antenna; theory; numerical modelling; measurements |
| **Abstract:** | This paper introduces an efficient analytical tool for the design of quasi-uniform acoustic leaky-wave antennas (ALWAs) based on circular holes perforated along the broad wall of a rectangular acoustic waveguide, together with experimental validation in terms of frequency-scanning capability. The analytical formulation combines the Transverse Equivalent Network (TEN) and the Transverse Resonance Equation (TRE) to predict leaky-mode dispersion parameters, including the phase constant and leakage rate. Compared to previously reported metamaterial-based ALWAs, which rely on complex resonant unit cells and exhibit limited scanning performance, the proposed structure provides a simpler alternative while maintaining effective beam-steering capability. The proposed approach bridges the gap between theoretical modeling and practical implementation, establishing a robust framework for the design and optimization of compact and cost-effective ALWAs suitable for acoustic sensing, communication, and localization applications. |
| **Additional Information:** | |
| **Question** | **Response** |
| Please read the Transfer of Copyright Agreement and the Instructions. By selecting the appropriate response below, you verify that you have consented to the Transfer of Copyright Agreement (if applicable) and the conditions and representations set forth in the Instructions. | O - Open Access (if you intend to pay the Open Access fee, select this option) |

# A quasi-uniform acoustic leaky-wave antenna: Analysis, design and experimental validation

Jens Forssén,[1, a] Pablo-Antonio Martínez-Vicente,[2] Astrid Algaba-Brazález,[2] Matthew Polidano,[1] and José-Luis Gómez-Tornero[2]

[1]*Division of Applied Acoustics, Department of Architecture and Civil Engineering, Chalmers University of Technology, SE-412 96 Gothenburg, Sweden*

[2]*Department of Communication and Information Technologies, Technical University of Cartagena, 30202 Cartagena, Spain*

(Dated: 6 March 2026)

This paper introduces an efficient analytical tool for the design of quasi-uniform acoustic leaky-wave antennas (ALWAs) based on circular holes perforated along the broad wall of a rectangular acoustic waveguide, together with experimental validation in terms of frequency-scanning capability. The analytical formulation combines the Transverse Equivalent Network (TEN) and the Transverse Resonance Equation (TRE) to predict leaky-mode dispersion parameters, including the phase constant and leakage rate. Compared to previously reported metamaterial-based ALWAs, which rely on complex resonant unit cells and exhibit limited scanning performance, the proposed structure provides a simpler alternative while maintaining effective beam-steering capability. The proposed approach bridges the gap between theoretical modeling and practical implementation, establishing a robust framework for the design and optimization of compact and cost-effective ALWAs suitable for acoustic sensing, communication, and localization applications.

[a]jens.forssen@chalmers.se

## I. INTRODUCTION

Leaky-wave antennas (LWAs)[1–3] have been extensively investigated in the electromagnetic domain as progressive-wave structures capable of generating directive radiation patterns with simple feeding (source) arrangements and frequency-dependent beam scanning. Initially developed for microwave and radiofrequency applications, they were later extended to optics, where similar dispersive mechanisms enabled beam steering in integrated waveguides[4]. More recently, these principles have been adapted to acoustics, giving rise to acoustic leaky-wave antennas (ALWAs), which transform frequency variations into controlled spatial beam scanning and enable direction finding without the need for complex phased arrays[5–8]. This property makes them attractive for scenarios where compactness, low cost, sustainability, and reduced hardware complexity are essential, since they enable angular estimation with a single microphone/loudspeaker rather than typical multi-element microphone/loudspeaker arrays, minimizing the number of transmit/receive (Tx/Rx) electronics.

Compared to traditional acoustic transducer arrays (microphone/loudspeaker arrays), which require multiple synchronized elements and complex control electronics, ALWAs can provide angular selectivity using a single excitation source and receiver. This results in significantly simpler, lighter, and more cost-effective architectures suitable for acoustic direction finding, source localization, and communication systems[5,9–11]. Their ability to perform frequency-to-angle mapping enables direct estimation of the direction of arrival with a single microphone when combined with appropriate signal-processing algorithms, as previously demonstrated in electromagnetic LWAs for localization and sensing[12–14]. These attributes make ALWAs particularly attractive for resource-constrained scenarios such as robotic navigation, structural monitoring, and autonomous sensing in the Internet of Things (IoT). Recently, the use of acoustic localization of WiFi devices has been experimentally demonstrated[15]. In addition, ALWAs have also been proposed as acoustic dispersive prisms, devices capable of separating different frequency components of a broadband signal into distinct angular directions[9], opening perspectives for applications in spectral analysis and acoustic imaging.

Several types of ALWAs have been reported, demonstrating different approaches to achieve acoustic beam steering, mainly based on acoustic metamaterials. In particular, some designs introduced periodic metamaterial-based unit cells incorporating resonant inclusions such as membranes or Helmholtz resonators to engineer the structure's dispersion, thereby controlling the beam direction as a function of frequency and, in some cases, achieving composite right/left-handed (CRLH) behavior[10,16–18]. These configurations enable backward-to-forward beam scanning across wide angular sectors.

Despite these advances, periodic and metamaterial-based ALWAs still face significant challenges such as manufacturing complexity, strong viscothermal losses, and narrow operating bandwidths, which limit their experimental performance and practical applicability[19]. Moreover, many prototypes have shown restricted scanning ranges and have failed to demonstrate consistent radiation across the full predicted angular span[5,16,20]. For example, a metamaterial-based ALWA employing a cylindrical waveguide with periodic modifications

was numerically proposed in Ref.[20], but its experimental validation of the proof-of-concept was not fully demonstrated. The lack of proper laboratory settings, including an acoustic anechoic chamber, may have reduced the reliability of the reported radiation patterns. Furthermore, only a limited set of measurement angles was recorded, preventing a clear reconstruction of the beam shape and sidelobe levels, thus limiting the evidence for frequency-scanning performance in spatial localization tasks. Consequently, although simulations often predict broadband scanning, the experimental evidence of ALWAs has so far remained inconclusive.

Recent efforts have attempted to address the challenges of practical ALWA implementations (complex configurations, narrow beam-scanning angles, limited bandwidth, manufacturing difficulties, etc.) by introducing heterogeneous loading strategies, where the acoustic impedance is spatially varied along the waveguide to improve directivity and scanning range[8]. However, most of these approaches still rely on periodic or complex metamaterial configurations whose analytical treatment is computationally demanding. The analysis of metamaterial-based ALWAs is typically performed using full-wave numerical simulations such as the finite element method (FEM)[21], which, although accurate, is computationally intensive and unsuitable for iterative design.

Alternatively, uniform and quasi-uniform ALWAs, in which acoustic leakage is achieved through non-resonant apertures such as slits or holes, offer a simpler and more scalable solution than metamaterial-based counterparts. This type of antennas has been extensively investigated in the electromagnetic domain, where introducing gradual variations along the aperture geometry through slits[1,22] or holes[23,24] enables improved control of both the leakage rate and beam scanning direction. Although conceptually simple, their theoretical and experimental study in acoustics remains limited and has not been explored in detail in the literature. Analytical formulations based on the Transverse Equivalent Network (TEN) and Transverse Resonance Equation (TRE), well established in the electromagnetic domain[22,25–28], provide a highly-efficient alternative to full-wave simulation. These techniques capture the key physical behavior of leaky modes using compact circuit-based representations, drastically reducing computational cost. Extending such methods to the acoustic field can therefore enable faster and more accurate design methodologies for uniform and quasi-uniform ALWAs.

In this work, a quasi-uniform ALWA is theoretically analyzed, designed, and experimentally validated. The proposed structure consists of a rectangular acoustic waveguide with an array of circular perforations along its broad wall, acting as controlled leakage points. For the first time in acoustics, an analytical framework based on the TEN and TRE methods is developed and applied to a quasi-uniform ALWA to predict its leaky-mode dispersion characteristics, including the phase constant (and consequent beam-scanning direction) and the leakage rate. The proposed model enables an efficient and physically insightful analysis of the complex leaky-mode behavior, providing results that agree closely with full-wave simulations obtained via finite-element modeling in Comsol Multiphysics, as well as with experimental measurements.

The paper is organized as follows: Section II introduces the theoretical framework for acoustic leaky-wave antennas, including the waveguide formulation and the TEN/TRE-based dispersion analysis used to predict the radiation angle and leakage rate. Section III describes the methodology adopted for the study, including the theoretical implementation, finite-element modeling, and the design of the experimental prototype and the measurement setup. Section IV presents the results obtained from theoretical predictions, numerical simulations, and experimental measurements, together with a comparison between them. Finally, Section V summarizes the main conclusions and discusses potential extensions toward more advanced acoustic leaky-wave antenna designs.

## II. THEORY

### A. Acoustic waveguides

The sound pressure in a rectangular acoustic waveguide open in $z$-dimension and with rigid walls in $x$ and $y$-dimensions can be formulated as[29]

$$\begin{aligned} p_{nm} &= \sum_{n,m} A_{nm} \cos\left(k_{xn}x\right) \cos\left(k_{ym}y\right) e^{j(\omega t - k_z z)} \\ k_0^2 &= k_{xn}^2 + k_{ym}^2 + k_z^2, \quad k_0 = \frac{\omega}{c} \\ k_z &= \left[\left(\frac{\omega}{c}\right)^2 - \left(k_{xn}^2 + k_{ym}^2\right)\right]^{\frac{1}{2}} \\ k_{xn} &= \frac{n\pi}{W}, \qquad n = 0, 1, 2, \ldots \\ k_{ym} &= \frac{m\pi}{H}, \quad m = 0, 1, 2, \ldots \end{aligned} \tag{1}$$

Here, $A_{nm}$ is the amplitude of the mode ($n$,$m$), $W$ and $H$ are the lengths of the cavity in dimensions $x$ and $y$, respectively, $t$ is time, $\omega$ is the angular frequency, $c$ is the sound speed, and $k_{xn}$ and $k_{ym}$ represent the wavenumbers for the axis and mode specified by the subscript. Here, it is assumed that the source is located at $z = 0$ and that the acoustic energy propagates in the positive $z$-direction.

If $k_0^2 = (\frac{\omega}{c})^2$ is larger than $k_{xn}^2 + k_{ym}^2$, the value of $k_z$ is real and there is propagation in the positive $z$-direction. If, on the other hand, $k_0^2$ is smaller than $k_{xn}^2 + k_{ym}^2$, the value of $k_z$ is imaginary, corresponding to an exponentially decaying field along the $z$-axis. The transition is the cut-off frequency of mode ($n$,$m$), given by[29]

$$\omega_{nm} = ck_{nm} = c\sqrt{k_{xn}^2 + k_{ym}^2}. \tag{2}$$

If the waveguide is excited at a certain driving frequency, all modes with a cut-off frequency below the driving frequency may propagate in the waveguide, whereas all modes with a cut-off frequency higher than the driving frequency will decay exponentially[29]. In the following,

we will assume that the height of the waveguide, $H$, is sufficiently small such that the working frequency range of interest will only allow propagating modes with $m = 0$, i.e., the wavenumber in $y$-direction is zero.

### B. Quasi-uniform leaky wave antenna

Introducing perforations, or other impedance changes, on the waveguide wall at $x = W$ allows radiation to the outside, for which the pressure field can be written as[10,20]

$$p(x, z) = p_0 e^{-jk_x x} e^{-jk_z z} \tag{3}$$

where the propagation angle is shown in Fig. 1. It is assumed that the perforations are densely spaced in comparison to the acoustic wavelength so that the effective impedance can be modeled as uniform, i.e., a quasi-uniform leaky-wave antenna.

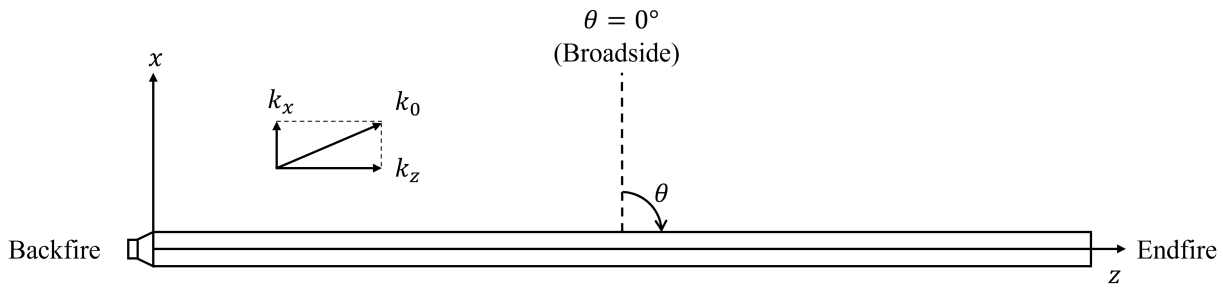


FIG. 1: Defining the directions for the acoustic leaky-wave antenna.

The wavenumber $k_z$ will generally be complex and can be written as $k_z = \beta - j\alpha$[20], where the leakage factor $\alpha$ and the propagation constant $\beta$ are the two fundamental parameters for the design of an acoustic leaky-wave antenna (ALWA)[30]. For $|\beta|$ smaller than $k_0$, the real part of $k_x$ becomes larger than zero, and radiation occurs[10,30], i.e., we have an ALWA.

### C. Radiation angle and leakage factor

The propagation constant, $\beta$, determines the angle of radiation, given by[10,20,30]

$$\theta = \sin^{-1}\left(\frac{\beta}{k_0}\right). \tag{4}$$

The leakage factor, $\alpha$, determines the amount of radiation per unit length[30], assuming that other losses are negligible, e.g., those due to viscous friction at openings. Assuming a reflection-free termination at the end of the antenna, the leakage factor can be calculated from[10]

$$\Psi_2 = \Psi_1 e^{-2\alpha l_{12}} \tag{5}$$

where $\Psi_1$ and $\Psi_2$ are the powers through an interior cross-section of the antenna at two locations separated by a distance $l_{12}$, which gives

$$\alpha = \frac{1}{2l_{12}} \ln\left(\frac{\Psi_1}{\Psi_2}\right). \tag{6}$$

The radiated power is associated with the active part of the leakage factor and is given by the real part of the complex-valued power. The reactive power is not contributing to the leaky-wave radiation but is associated with power that is reflected back to the source[31,32]. The instantaneous acoustic power in a cross-section of the antenna cavity can be calculated for a single-frequency sound field as[33]

$$\Psi = \int_S \mathbf{I}_c \cdot \hat{\mathbf{z}}\, dS \tag{7}$$

$$\mathbf{I}_c = \frac{1}{2} p \mathbf{u}^* \tag{8}$$

where $S$ is the area of the cross-section of the antenna parallel to the $xy$-plane, $\hat{\mathbf{z}}$ is the unit vector in the $z$-direction, $I_c(x, y)$ is the instantaneous complex intensity, $p$ is the complex pressure, $\mathbf{u}$ is the complex particle velocity, and $^*$ denotes the complex conjugate. When taking the time-average of $I_c$, the imaginary part vanishes, leaving only the contribution of the active intensity[33]. Using the specific acoustic impedance, defined as the ratio of pressure and particle velocity, $Z^{\mathrm{s}}_{0,z} = \frac{p}{\mathbf{u}\cdot\hat{\mathbf{z}}}$, with $Z^{\mathrm{s}}_{0,z} = \frac{\rho_0 \omega}{k_z}$, where $\rho_0$ is the air density, we get

$$\mathbf{u}^* \cdot \hat{\mathbf{z}} = \frac{p^* k_z^*}{\rho_0 \omega}. \tag{9}$$

Ursing $k_z^* = \beta + j\alpha$ and Eqs. (7–9), the instantaneous power at the source can be calculated as

$$\Psi(0) = \frac{(\beta + j\alpha)}{2\rho_0 \omega} \int_S |p|^2\, dS. \tag{10}$$

From Eq. (5), the power at distance $z$ from the source can be expressed as

$$\Psi(z) = \Psi(0) e^{-2\alpha z}. \tag{11}$$

The leakage factor can be found through differentiation of the power expression (11) with respect to $z$[32]:

$$-\frac{\mathrm{d}\Psi(z)}{\mathrm{d}z} = 2\alpha \Psi(0) e^{-2\alpha z} \tag{12}$$

i.e.,

$$-\frac{\mathrm{d}\Psi(z)}{\mathrm{d}z} = 2\alpha \Psi(z). \tag{13}$$

Upon studying the real part of this, the active component of $\alpha$ can be identified as[31]

$$\alpha_{\text{active}} = \frac{\mathrm{Re}\left[-\frac{\mathrm{d}\Psi(z)}{\mathrm{d}z}\right]}{2|\Psi(z)|} \tag{14}$$

which can also be written as

$$\alpha_{\text{active}} = \alpha \frac{\beta}{\sqrt{\alpha^2 + \beta^2}}. \tag{15}$$

The corresponding formulation for the reactive part can be written as

$$\alpha_{\text{reactive}} = \alpha \frac{\alpha}{\sqrt{\alpha^2 + \beta^2}} \tag{16}$$

such that $\alpha^2_{\text{active}} + \alpha^2_{\text{reactive}} = \alpha^2$ is fulfilled. In the results from the theoretical solution we will, due to convention, plot the total leakage factor:

$$\alpha = \frac{\left|\frac{\mathrm{d}\Psi(z)}{\mathrm{d}z}\right|}{2|\Psi(z)|}. \tag{17}$$

### D. Design parameters of an acoustic leaky-wave antenna (ALWA)

A simple design of a uniform ALWA is a rectangular waveguide with a slit-perforation on one side. Here, a series of circular holes is used instead of a slit, making the antenna fulfill a quasi-uniform design provided that the periodic spacing is much smaller than the wavelength. The geometry of such an ALWA design is shown in Fig. 2 where the propagation inside the antenna is in the $z$-direction, perpendicular to the $xy$-plane. The source is located at one end of the ALWA ($z = 0$) and at the opposite end ($z = L$) a reflection-free termination is assumed. The length of the ALWA, $L$, needs to be significantly larger than the wavelength of the lowest operating frequency.

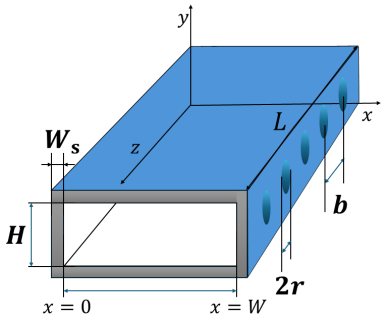


FIG. 2: Geometry of the acoustic leaky-wave antenna.

The pressure of the sound waves in the $x$-direction of the ALWA can be modeled as a linear combination of waves, formulated as[29]

$$p(x,t) = Ae^{j[\omega t + k_x(W-x)]} + Be^{j[\omega t - k_x(W-x)]} \tag{18}$$

where $A$ and $B$ are the amplitudes of the forward and backward traveling waves, respectively. To find a relation between $A$ and $B$, the boundary conditions for pressure and particle

177 velocity are used. The relation between particle velocity and pressure is given by[29]

$$u(x,t) = -\frac{1}{\rho_0}\int \frac{\partial p}{\partial x}\,dt \tag{19}$$

178 which gives

$$u(x,t) = -\frac{1}{j\omega\rho_0}\cdot\frac{\partial p}{\partial x}. \tag{20}$$

179 Inserting this into Eq. (18) gives

$$u(x,t) = \frac{1}{\omega\rho_0}\left[Ak_x e^{jk_x(W-x)} - Bk_x e^{-jk_x(W-x)}\right]e^{j\omega t}. \tag{21}$$

180 Using the impedances at the left and right walls, $Z_L = \frac{p(0,t)}{u(0,t)}$ and $Z_R = \frac{p(W,t)}{u(W,t)}$, respectively,
181 we can write:

$$Z_L = \frac{\omega\rho_0}{k_x}\cdot\frac{\left(Ae^{jk_xW} + Be^{-jk_xW}\right)}{\left(Ae^{jk_xW} - Be^{-jk_xW}\right)} \qquad \text{at } x = 0 \tag{22}$$

182

$$Z_R = \frac{\omega\rho_0}{k_x}\cdot\frac{(A+B)}{(A-B)} \qquad \text{at } x = W. \tag{23}$$

183 With $Z_{0,x} = \rho_0\omega/k_x$, the characteristic impedance of the ALWA in the $x$-direction, we get

$$Z_R = Z_{0,x}\cdot\frac{A+B}{A-B} \tag{24}$$

184 which, inserted in Eq. (23), gives

$$A = B\cdot\frac{Z_R + Z_{0,x}}{Z_R - Z_{0,x}}. \tag{25}$$

185 Using Eq. (25) in Eq. (22) results in

$$Z_L = Z_{0,x}\cdot\frac{B\frac{Z_R+Z_{0,x}}{Z_L-Z_{0,x}}e^{jk_xW} + Be^{-jk_xW}}{B\frac{Z_R+Z_{0,x}}{Z_L-Z_{0,x}}e^{jk_xW} - Be^{-jk_xW}} \tag{26}$$

186 which can be simplified to

$$Z_L = \frac{Z_R + jZ_{0,x}\tan(k_xW)}{1 + j\frac{Z_R}{Z_{0,x}}\tan(k_xW)}. \tag{27}$$

187 If the wall at $x = 0$ is rigid, the boundary condition must meet $u(0,t) = 0$, i.e.,

$$k_x(Ae^{jk_xW} - Be^{-jk_xW}) = 0 \tag{28}$$

188 which gives

$$A = Be^{-2jk_xW}. \tag{29}$$

189 Insertion of Eq. (29) into Eq. (23), results in

$$Z_R = Z_{0,x} \cdot \frac{e^{-jk_xW} + e^{jk_xW}}{e^{-jk_xW} - e^{jk_xW}} \tag{30}$$

which equates to

$$Z_R = -jZ_{0,x} \cot(k_xW). \tag{31}$$

Solving for $k_x$ gives

$$k_x = \frac{1}{W} \cdot \left[ \arctan\left( j\frac{Z_{0,x}}{Z_R} \right) + n\pi \right], \quad n = 0, 1, 2, \ldots \tag{32}$$

Equation (32) for $k_x$ is similar to the case of the closed waveguide, but contains an additional term $\arctan(jZ_{0,x}/Z_R)$, due to the influence of the finite impedance wall. This additional term allows for a non-zero value of $k_x$ for the case where $n = 0$ and hence this allows for leaky-wave radiation for the (0,0) mode.

In the following, the (0,0) and (1,0) modes are studied. Since the impedances in Eq. (32) depend on $k_x$, the equation does not represent a closed-form solution. How to solve for $k_x$, and to find $k_z$, will be treated in Section II G.

### E. Predicting the mode shapes

The mode-shape, i.e., the shape of the pressure pattern in the cross-section of the antenna, can be found by substituting the expression found for $A$ in Eq. (29) into Eq. (18). Including also the dependence in the $y$-direction, from Eq. (1), the resulting equation for the pressure mode $(n,m)$ is

$$\begin{aligned} p_{n,m}(x,y) &= B\left(e^{-jk_{x,n}(W+x)} + e^{-jk_{x,n}(W-x)}\right)\cos\left(k_{y,m}y\right) \\ &= A_{nm}e^{-jk_{x,n}W}\cos\left(k_{x,n}x\right)\cos\left(\frac{m\pi}{H}y\right) \end{aligned} \tag{33}$$

where $k_{x,n}$ and $k_{y,m}$ denote $k_x$ and $k_y$ evaluated for mode $(n,m)$ and $A_{nm}$ is the amplitude of mode $(n,m)$. The total pressure is given by the sum of all the modes excited in the waveguide, i.e.,

$$p(x,y) = \sum_{n,m} A_{nm}e^{-jk_{x,n}W} \cos\left\{ \left[ \arctan\left( j\frac{Z_{0,x}}{Z_R} \right) + n\pi \right] \frac{x}{W} \right\} \cos\left(\frac{m\pi}{H}y\right) \tag{34}$$

where $k_x$ from Eq. (32) has been inserted. In Fig. 3 the modes $(0,0)$ and $(1,0)$ are plotted as function of $x$ using Eq. (33) with $f = 400$ Hz for $n = 0$ and $f = 1900$ Hz for $n = 1$, and normalizing by setting $A_{nm}\exp(-jk_{x,n}W) = 1$. The impedance model for $Z_R$ is described in Section II F . For the $n = 1$ mode, it is interesting to note that the zero-crossing of the real part is not centered along the $x$-direction. This may open for a possible optimization of the location of the excitation.

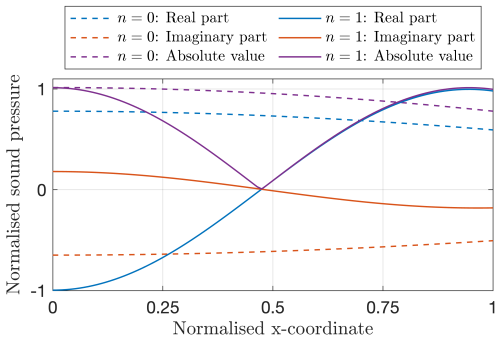


FIG. 3: Mode shapes for $n = 0$ and $n = 1$ exemplified for the antenna with circular perforations.

### F. Modelling the impedance for periodically spaced holes

The surface impedance of a circular hole is given by[34]

$$Z_S = j\omega\rho_e l, \qquad \rho_e = \rho_0 \left[1 - \frac{2}{s\sqrt{-j}} \frac{J_1(s\sqrt{-j})}{J_0(s\sqrt{-j})}\right]^{-1} \tag{35}$$

where $l$ is the neck-length of the cylindrical hole (i.e., $W_S$ in Fig. 2) and $s = r\sqrt{\frac{\omega\rho_0}{\mu}}$ where $r$ is the radius of the hole and $\mu$ is the coefficient of viscosity of air, which provides friction losses.

The radiation impedance of a circular hole at the end of a long tube for values of $kr < 0.5$ can be approximated as[35]:

$$Z_{11} = \frac{1}{4}\rho_0 c k_0^2 r^2 + 0.6134 j \rho_0 c_0 k_0 r. \tag{36}$$

The impedance at the end of a tube was chosen because for low frequencies, the baffle formed by the antenna is small compared to the wavelength and behaves similarly to a long tube. Furthermore, to account for both ends of the hole, the imaginary part of $Z_{11}$ is multiplied by two[36].

To obtain the specific impedance of the linear array of circular holes, it must be normalized by the porosity, $\phi$[36]. This can be calculated as the ratio of the area of a single hole to the area of the surface corresponding to that hole, i.e.,

$$\phi = \frac{\pi r^2}{bH} \tag{37}$$

where $b$ is the hole separation and $H$ is the height of the ALWA cavity as shown in Fig. 2.

Furthermore, the mutual impedance of adjacent holes should be considered. The mutual impedance of two identical holes with the same phase and amplitude is given by[37]

$$Z_{12} = R_{11}\left[\frac{\sin kb}{kb} + j\frac{\cos kb}{kb}\right] \tag{38}$$

where $R_{11}$ is the real part of the radiation impedance of a single hole and $k$ is the wavenumber. Considering a single hole with $N$ holes on either side with a hole spacing of $b$, the total impedance for this hole would be:

$$Z_r = Z_{11} + 2 \cdot \sum_{n=1}^{N} R_{11} \left[ \frac{\sin nkb}{nkb} + j \frac{\cos nkb}{nkb} \right]. \tag{39}$$

Since this equation is only valid if the radiators all have the same phase and amplitude, we will consider only the influence of the two closest holes. Hence, the total impedance is modeled as

$$Z_R = \frac{j\omega\rho_0 l}{\phi} \left[ 1 - \frac{2}{s\sqrt{-j}} \frac{J_1(s\sqrt{-j})}{J_0(s\sqrt{-j})} \right]^{-1} + \frac{\rho_0 c \left(k_0 r\right)^2}{4\phi} \left[ 1 + 2 \cdot \sum_{n=1}^{2} \left( \frac{\sin nkb}{nkb} + j \frac{\cos nkb}{nkb} \right) \right] + 2 \times 0.6134 j \frac{\rho_0 c}{\phi} kr. \tag{40}$$

### G. TEN/TRE formulation for leaky-mode dispersion

For the design of a leaky-wave antenna, it is useful to analyze the guided-mode propagation through the transverse cross section of the waveguide. To this end, we use the Transverse Equivalent Network (TEN), which represents the waveguide cross section as an equivalent circuit model (see Fig. 4), thereby reducing the original 3D guided-wave problem to a 1D transverse formulation. This approach makes it possible to efficiently determine suitable values of the design parameters in order to control the leakage rate and the frequency dependence of the scanning angle.

The circuit topology in Fig. 4 is inherited from the electromagnetic (EM) TEN/TRE formulation used for leaky-wave antennas, where the transverse field problem is mapped onto an equivalent transmission line section of length $W$ with a characteristic impedance $Z_{0,x}$. In that EM interpretation, the two long parallel lines in Fig. 4 correspond to the two conductors of the transmission-line representation, and the terminal loads $Z_L$ and $Z_R$ implement the boundary conditions through equivalent impedances (e.g. modeling the lateral guide walls and the openings)[38,39]. Here we use the same formalism in acoustics by working with the pressure/volume velocity variables ($Z = p/U$). Under this framework, the right hand side with the openings can be represented by an equivalent acoustic impedance $Z_R$ that models the wall with radiating surface openings where the mode leaks into the exterior air. The left hand side here models an acoustically hard surface with infinite impedance.

To analyze the TEN, a resonance condition is imposed on the reflection factors, yielding the Transverse Resonance Equation (TRE) in terms of the reflection coefficients[24,25]:

$$\overleftarrow{\rho} \cdot \rho_R = 1 \tag{41}$$

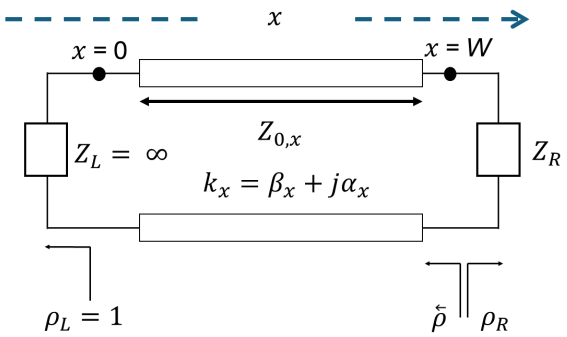


FIG. 4: General TEN model of the cross section for a rectangular acoustic waveguide with a lateral opening perturbation.

Here, $\rho_R$ is the complex reflection factor of the opening surface

$$\rho_R = |\rho_R|\, e^{j\psi_R} = \frac{Z_R - Z_{0,x}}{Z_R + Z_{0,x}} \tag{42}$$

and $\overleftarrow{\rho}$ is the effective reflection factor seen when looking from the opening toward the opposite side

$$\overleftarrow{\rho} = \rho_L\, e^{-j\,2k_x W} \tag{43}$$

where $\rho_L$ denotes the reflection factor at the left wall, which is modeled as a rigid boundary condition, i.e. $\rho_L = 1$.

The complex exponential term in Eq. (43) represents the phase accumulated during the one-way and return across the transmission line. Substituting Eqs. (42) and (43) into Eq. (41), we get, with $k_x = \beta_x + j\alpha_x$

$$|\rho_R| e^{j\psi_R} \cdot e^{-j2\beta_x W} \cdot e^{2\alpha_x W} = 1. \tag{44}$$

Rearranging terms leads to

$$e^{-j2\beta_x W} \cdot e^{2\alpha_x W} = \frac{1}{|\rho_R|} e^{-j\psi_R}. \tag{45}$$

This complex equation is satisfied by independently enforcing the phase and magnitude conditions. First, the phase condition requires

$$2\beta_x W = \psi_R + 2\pi n, \qquad n \in \mathbb{N} \tag{46}$$

where n is the transverse mode index arising from the $2\pi$ phase ambiguity of the resonance condition; each step in $n$ selects a higher-order transverse mode branch, which becomes propagating as the operating frequency increases above cut-off. This gives

$$\beta_x = \frac{\psi_R + 2\pi n}{2W}. \tag{47}$$

Second, the magnitude condition gives

$$\alpha_x = \frac{1}{2W} \ln\left(\frac{1}{|\rho_R|}\right). \tag{48}$$

Combining real and imaginary parts, the transverse wavenumber can be expressed as

$$k_x = \beta_x + j\alpha_x = \frac{\psi_R + 2\pi n}{2W} + j\frac{1}{2W} \ln\left(\frac{1}{|\rho_R|}\right). \tag{49}$$

From the above, we conclude that given an impedance model for the aperture surface, the transverse wavenumber can be determined.

Since $\rho_R$ depends on the characteristic impedance (Eq. 42), which depends on $k_x$, Eq. (49) becomes a transcendental equation of the form $k_x = F(k_x)$, which does not admit a closed-form solution. To solve for $k_x$, we define an objective function $M(k_x)$ to be numerically minimized

$$M(k_x) = |k_x - F(k_x)| \tag{50}$$

where $F(k_x)$ is the transcendental function obtained from Eq. (49):

$$F(k_x) = \frac{\psi_R(k_x) + 2\pi n}{2W} + j\frac{1}{2W} \ln\left(\frac{1}{|\rho_R(k_x)|}\right). \tag{51}$$

Since $M(k_x)$ may exhibit multiple local minima, optimization is initialized with an analytical estimate of $k_x$, obtained by evaluating Eq. (49) with the plane-wave characteristic impedance $Z_0 = \omega\rho_0/k_0$, which makes $\rho_R$ independent of $k_x$ in Eq. (42) and provides a robust starting point. Once the transverse wavenumber $k_x$ is obtained from the numerical solution of the TRE, the associated complex longitudinal wavenumber $k_z$ is given by $k_z = \sqrt{k_0^2 - k_x^2}$. Due to the assumption $H < \lambda/2$, the modes are taken to be invariant along the $y$ direction, which implies $k_y = 0$.

We next recall the standard leaky-wave relations used to quantify the radiation performance of an ALWA. From the complex longitudinal wavenumber of the leaky mode

$$k_z = \beta - j\alpha \tag{52}$$

the phase constant $\beta$ determines the main-beam scanning angle (measured from broadside), while the leakage rate $\alpha$ governs the longitudinal power decay. In particular, the beam direction can be approximated by[24]:

$$\theta(f) \approx \arcsin\left(\frac{\beta(f)}{k_0}\right) \tag{53}$$

and the half-power beamwidth of a uniformly excited effective aperture can be estimated as[24]:

$$\Delta\theta \approx \lambda_0 \frac{57^\circ}{L} \frac{1}{\cos\theta}. \tag{54}$$

Using the above solution, the radiation behavior of the ALWA is conveniently characterized by the frequency–beam scanning curve $\theta(f)$ together with the normalized leakage curve $\alpha(f)/k_0$.

## III. METHOD

### A. Theoretical solution

| Parameter | Value |
|---|---|
| $H$ (ALWA cavity height) | 35 mm |
| $W$ (ALWA cavity width) | 95 mm |
| $L$ (ALWA length) | 1.5 m |
| $W_s$ (wall thickness) | 2.5 mm |
| $r$ (hole radius) | 4 mm |
| $b$ (hole separation) | 30 mm |

TABLE I: Geometric parameters of the prototype antenna used for validation.

A quasi-uniform ALWA with dimensions listed in Table I is studied using the proposed TRE method. The TEN, which applies the transverse resonance condition, is implemented in Matlab to solve Eq. (50) for $k_x$ using the `fminsearch` function[40] to minimize the objective function $M(k_x)$. The resulting solution is then used to compute the radiation angle,$\theta$, and the normalized leakage rate $\alpha/k_0$.

A parametric study was performed varying the radius, $r$, and width, $W$. The resulting dispersion curves, which are obtained by varying a single design parameter at a time, the hole radius $r$ or the waveguide width $W$, are reported in Figs. 5 and 6 respectively. Two modes are shown in both figures, the mode $n = 0$ which inherently exists and can propagate longitudinally without cut-off, and mode $n = 1$ which is analogous to the first higher-order transverse variation (referred to as the $TE_{10}$ mode for rectangular electromagnetic waveguides).

We analyze the evolution of both modes in Fig. 5 as the hole radius approaches zero. As plotted in Fig. 5a, mode $n = 0$ converges to the longitudinal closed-waveguide limit, yielding endfire radiation ($\theta = 90°$) across the entire frequency range, and a vanishing radiation leakage rate, as confirmed in 5b. This is consistent with the fact that the mode $n = 0$ in a closed waveguide reduces to a plane wave with no leakage, propagating only along the z-axis and remaining uniform across the transverse direction. As the hole radius increases, the waveguide transitions to a leaky configuration and the $n = 0$ mode becomes radiative. However, the scanning angle, $\theta$, and the attenuation rate, $\alpha/k_0$, change abruptly,

indicating a limited controllability of its radiation characteristics, shown in both Figs. 5 and 6.

In contrast, the mode $n = 1$ has an onset frequency around 1800 Hz, as seen in Figs. 5 and 6, consistent with the closed-waveguide cut-off frequency of the higher order mode in a conventional rectangular waveguide. For a very small hole radius (see Fig. 5), the solution for $n = 1$ approaches the closed-waveguide limit. When the radius increases, so does the attenuation rate (Fig. 5a), as expected, but the mode preserves essentially the same dispersion curve, i.e., $\theta$ varies smoothly (Fig. 5b), in contrast to the mode $n = 0$, which exhibits an abrupt transition when the opening is introduced.

As shown in Fig. 6a, as $W$ increases, the dispersion curves are shifted in frequency, in a more pronounced way for the $n = 1$ mode than for the $n = 0$ mode. By comparing Figs. 5a and 6a, it can be observed that the onset frequency of the angular scanning is more sensitive to changes in $W$ than in $r$ for $n = 1$. This behavior can be explained by the transverse resonance condition for $n = 1$, where the phase shift due to $W$ is typically much larger than the phase shift due to $\psi_R$. This is further supported by Fig. 6a, where the radiation curves of the $n = 1$ mode remain very close to those of the closed-waveguide case, for which $\beta_x = \pi/W$. Thus, $W$ mainly controls the transverse phase constant and the corresponding frequency shift, and therefore the scanning angle. Conversely, comparing Figs. 5b and 6b, we can see that at a fixed frequency, the leakage rate is more sensitive to changes in $r$ than in $W$. This provides a good mechanism for controlling $\alpha$ and $\theta$ by selecting $r$ and $W$ for a desired level of leakage and radiation angle, respectively.

An additional insight can be drawn from Fig. 6a by comparing the $n = 1$ scanning-angle curves with those for the closed-waveguide condition (CW). Only a slight frequency shift is observed compared to having openings, whereas the dispersion trend is practically preserved. This provides a useful tool for rapidly estimating the ALWA behavior using only the closed-waveguide expression. In other words, a first-order prediction of $\theta$ can be obtained without solving the TRE and its associated transcendental equation. On the other hand, the closed waveguide approximation is not applicable to the mode $n = 0$, since in the closed case it reduces to a plane-wave solution ($k_z \approx k_0$); consequently, the closed waveguide dispersion for $n = 0$ does not provide a meaningful reference to predict the open (leaky) behavior.

From these initial simulations, we conclude that the $n = 1$ leaky mode is more suitable for ALWA applications than the $n = 0$ leaky mode. For the $n = 1$ mode, the scanning angle, $\theta$, and the normalized leakage rate, $\alpha/k_0$, can be controlled smoothly by adjusting the radius, $r$, and the width of the waveguide, $W$, where $r$ primarily controls leakage, while $W$ controls beam scanning. This contrasts to the mode $n = 0$ which exhibits an abrupt transition from a closed mode to a leaky case, a characteristic that limits its practical controllability.

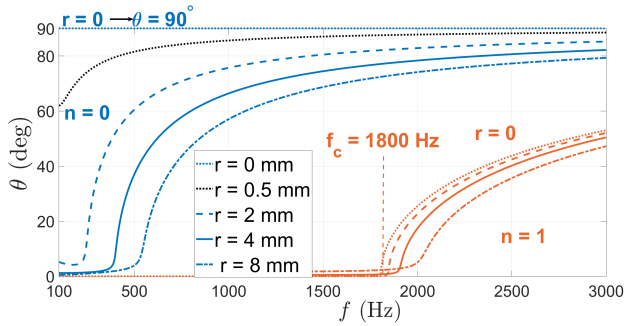


(a) Frequency scanning-angle $\theta$ for the $n = 0$ (blue curves) and $n = 1$ modes (orange curves).

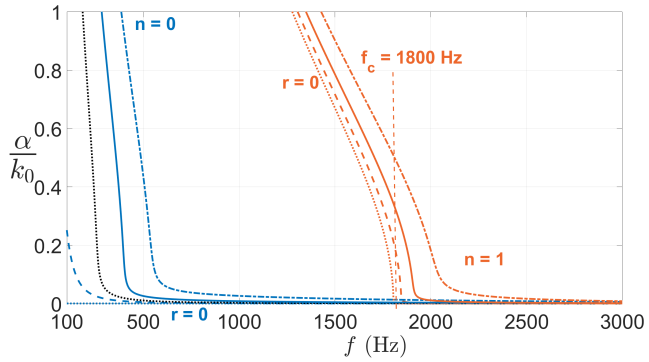


(b) Attenuation-rate behavior for the $n = 0$ (blue curves) and $n = 1$ modes (orange curves).

FIG. 5: Leaky-mode dispersion curves obtained for a quasi-uniform ALWA, as the aperture radius $r$ varies. Including the closed-waveguide limit ($r \Rightarrow 0$).

### B. Finite element modelling

To validate the theoretical model, Finite Element Method (FEM) calculations were carried out in Comsol Multiphysics (version 6.2) using the *Pressure Acoustics, Frequency Domain* interface. The geometry was defined in Comsol by creating the shape of the air inside the antenna and in a volume surrounding it, with the solid material of the ALWA assumed to be a perfectly rigid material. As outer boundary, a sphere, truncated on top, bottom, and backside to reduce computation time, was used. By trial and error, the minimum size of the sphere and the amount of truncation were found, not significantly affecting the results of the simulation (see Fig. 7).

The outer boundary of the truncated sphere used the Perfectly Matched Boundary (PMB) condition to suppress reflections[41]. These surfaces also enable External Field Calculation, used for extrapolating the sound field outside the model to compute far-field directivity[42]. All ALWA walls except at the source and termination were treated as rigid, fully reflective boundaries[43]. The termination wall was given a PMB condition to model the ideal case of reflection-free termination. For exciting the (0,0) mode in the ALWA, a velocity source

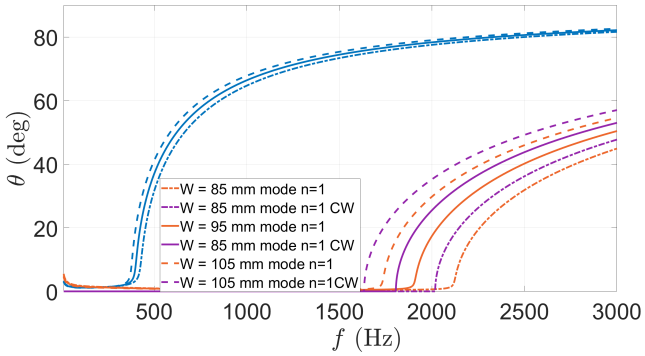


(a) Frequency scanning angle $\theta$ for the $n = 0$ modes (in blue) and the $n = 1$ modes (in orange), including also the results for the $n = 1$ mode of a closed waveguide (CW) (in purple).

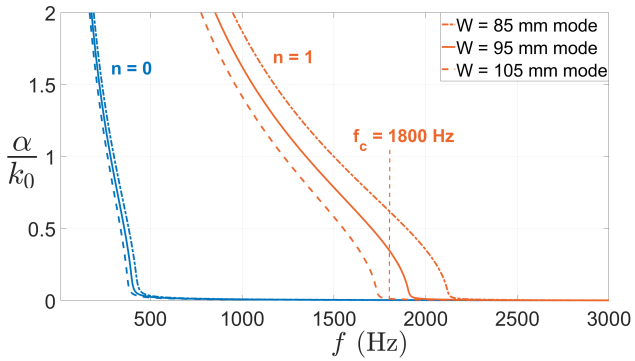


(b) Attenuation-rate behavior for the $n = 0$ (blue curves) and $n = 1$ modes (orange curves).

FIG. 6: Leaky-mode dispersion curves obtained for a quasi-uniform ALWA, as the width of the waveguide $W$ varies.

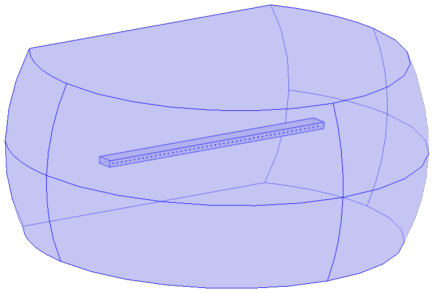

FIG. 7: Comsol model showing the truncated sphere used as outer boundary in relation to the antenna. (The outer boundary has a diameter of 2.4 m and a height of 1 m.)

condition was imposed on the whole of the source wall, with a chosen velocity amplitude of 0.1 m $s^{-1}$. To instead excite the (1,0) mode to a larger extent than the (0,0) mode, the source wall is split into two halves; one half with a velocity of 0.1 m $s^{-1}$ and the other half

with a velocity of $-0.1\ \mathrm{m\ s^{-1}}$. These two source settings simulate a theoretical monopole and dipole, respectively. Note that the numeric value of the amplitude can be chosen arbitrarily since it does not affect the final results in terms of radiation angle and leakage rate.

The mesh was constructed in Comsol as free tetrahedral quadratic Lagrange elements with a frequency-varying size of 1/5 of the wavelength. This degree of refinement is generally considered sufficient and is also confirmed by comparing the results with the theoretical predictions. Modeling of viscous effects was not included here, which may need further mesh refinement.

The resulting sound pressure level directivity patterns were generated in Comsol from the External Field Calculation and exported as a text file. Imported to Matlab, the angle of the main lobe was estimated taking the maximum value of each directivity pattern, restricted to angles between 0° and 90° to avoid capturing the lobe on the back of the antenna.

The leakage rate estimate was based on power flows through cross-sectional planes of the ALWA cavity positioned close to the source and close to the termination. These quantities were inserted into Eq. (5), with the power flow at each plane obtained by surface integration of the active acoustic intensity output from Comsol.

## C. Prototype construction and experimental setup

### *1. Manufacturing the acoustic leaky-wave antenna*

The ALWA was manufactured from a rectangular aluminum tube with dimensions listed in Table I. The dimensions were chosen to mainly prioritize good measurement quality for the (1,0) mode with a cut-off frequency estimated at 1800 Hz and the onset of the frequency-scanning behaviour being around 1900 Hz (see Fig. 6a ).

To make the ALWA operate in radiating mode, two loudspeaker elements were used as acoustic source. A plastic fixture for the loudspeakers was 3D-printed (see Fig. 8), to be attached to the source end of the tube and sealed with tape.

To approximate a reflection-free termination, a sample of mineral wool was placed inside the end of the tube. In addition, a fully reflecting termination was used, approximated by attaching a cut aluminum plate to the end of the tube and sealing with tape.

FIG. 8: Loudspeakers and loudspeaker fixture.

### 2. *Measurement method*

The measurements were made in an anechoic chamber with an external control room. A measurement computer supplied the output signal to the loudspeakers (Visaton BF 32 S WP), via a power amplifier (Fosi Audio ZA3), and received the signals from two measurement microphones (GRAS 46AF) via a microphone amplifier (GRAS Power Module Type 12AA). A loop-back connection was made from the output of the audio interface to an input channel, enabling a direct measurement of the loudspeaker's input signal.

The power amplifier was used in mono mode and connected to an in-house built phase switch inside the anechoic chamber, which provides two output signals for two loudspeakers. Using the *monopole* setting of the switch, both loudspeakers are fed with the same signal in phase, whereas using the *dipole* setting, one of the loudspeakers is fed with the original input signal while a phase difference of 180° is applied to the other.

The antenna was placed on a rotating table (Varisphear) in an anechoic chamber, as shown in Figs. 9 and 10. A Matlab program on the measurement computer was used to control the rotation in steps of 1° and to perform an impulse response measurement at each angle using the swept-sine technique (e.g.[44]). An FFT was performed on the measured impulse response at each angle to obtain the directivity of the antenna through the magnitude of the frequency response function.

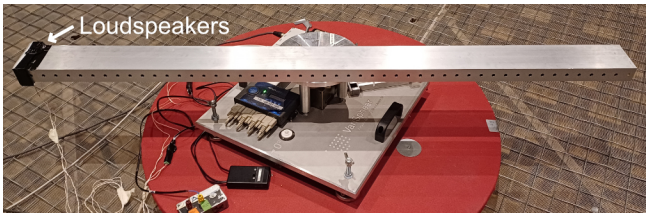


FIG. 9: The prototype antenna with attached loudspeakers, placed on the turntable.

Measurement data were collected for four different microphone positions placed at a 3–5 m distance from the center of the antenna (using two microphones at a time), repeated for the four combinations of termination (absorber or reflector) and source type (monopole or dipole).

The measured directivities were used to determine the radiation angle by finding the angle of the maximum magnitude in the same way as for the Comsol simulation results.

The leakage rate was estimated using the measurements with the reflector termination, as[45]

$$\frac{\alpha}{k_0} = \frac{G_{fwd} - G_{bwd}}{k_0 \cdot 20L \log_{10}(e)} \tag{55}$$

where $G_{fwd}$ and $G_{bwd}$ are the gains of the forward and backward lobes in dB, respectively.

The radiation angle and leakage rate obtained from each microphone position were averaged and the uncertainty of the mean values in terms of a 95 % confidence interval is

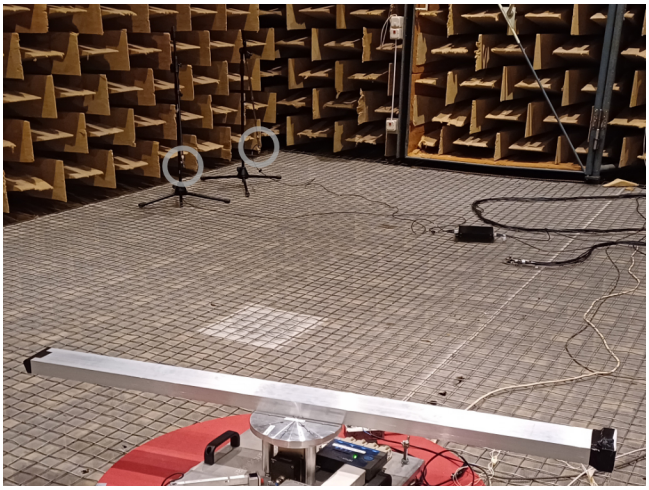

FIG. 10: The prototype antenna in the anechoic chamber. The measurement microphones are marked by gray circles.

estimated as $u = ts/\sqrt{n}$ where $s$ is the experimental standard deviation, $n$ is the number of measurements, and $t$ is determined from Student's $t$-distribution; $t = 3.18$ for $n = 4$ and 95 % confidence interval. The uncertainty of the initial angle of the antenna was estimated to be about 2°.

## IV. RESULTS

### A. Resulting pressure fields from finite-element modeling

Calculations using finite-element modeling in Comsol were carried-out for both monopole and dipole excitations to study the (0,0) and the (1,0) modes. Figure 11 illustrates the acoustic pressure field for the dipole excitation at three different frequencies. In Fig. 11a the frequency (1500 Hz) is below the cut-off of the (1,0) mode, whereby the response corresponds to that of the (0,0) mode, showing a plane-wavelike sound field inside the antenna. Figure 11b shows the result at 2000 Hz, which is above the cut-off of the (1,0) mode. A dipole pattern is visible inside the antenna, which confirms that the (1,0) mode is mainly excited. Outside the antenna, the radiation shows a clear directionality of the sound field, as expected for operation above cut-off. In addition, the strength of the radiated sound field is much larger than in Fig. 11a, where the leakage rate is significantly higher. When further increasing the frequency to 2500 Hz (Fig. 11c), the direction of the radiated sound field shifts further toward end-fire, as expected.

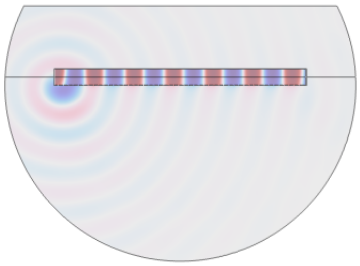

(a) $f = 1500$ Hz.

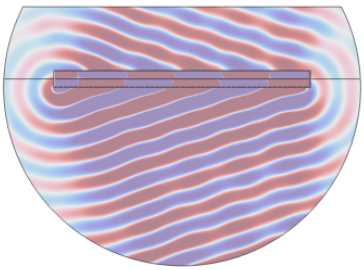

(b) $f = 2000$ Hz.

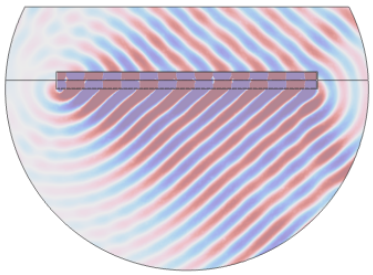

(c) $f = 2500$ Hz.

FIG. 11: Plots of the acoustic pressure amplitude (real part) for the antenna operated with a dipole source.

## B. Results from theoretical modeling, finite-element modeling, and measurements

### *1. Radiation angle and leakage rate as function of frequency*

The resulting radiation angle and leakage rate as function of frequency are plotted in Figs. 12–15 based on theoretical modeling, finite-element modeling, and measurements of the designed prototype leaky-wave antenna operated by a monopole and a dipole source. The procedure used to determine the radiation angle and leakage rate for each method is described above in the corresponding section.

Comparing the radiation angle results from the theoretical (Theory) and finite-element modeling (Comsol), in Figs. 12 and 14, a very good agreement is shown, thus successfully validating the finite-element modeling. The results for the monopole source (Fig. 12) show an abrupt increase in the radiation angle, starting at about 400 Hz. In contrast, the results for the dipole source (Fig. 14) show a more gradual increase in radiation angle as the frequency increases from the onset (at about 1900 Hz) and above, as expected from the theoretical results.

The agreement between the modeled leakage rates obtained from theory and finite-element simulations (Figs. 13 and 15) is good at higher frequencies but deviates in the frequency range where the leakage rate peaks and below, concluded to be due to the finite resolution of the numerical solution.

Concerning the measured results, they are plotted as mean value and estimated 95 % confidence interval in Figs. 12–15. The agreement in radiation angle, with both theory and numerical results, is excellent for the dipole source (Fig. 14) and very good for the monopole source at higher frequencies, above approximately 1500 Hz (Fig. 12). In the lower frequency range of 300–1000 Hz, the agreement for the monopole source is good in terms of the measured mean value; however, individual measurements show large discrepancies, as reflected by the large uncertainty. This behavior can be attributed to resonances along the length of the antenna, which are allowed to be excited due to the lack of a reflection-free termination in the measurement setup. At about 975 Hz a large deviation from the modeled radiation angle is observed in the measured results. The reason for this is not fully understood, but may be related to a quarter-wavelength resonance in the antenna cross-section.

The measured leakage rates generally show very good agreement with the modeled results at higher frequencies (Figs. 13 and 15). In the low-frequency ranges discussed above for the monopole radiation-angle results, the measured leakage rate also deviates. In addition, near the peak of the leakage rate, the measured data also deviate from the theoretical results. This is mainly attributed to measurement uncertainties, which become more influential in leakage-rate estimation because it involves a difference operation (see Eq. 55).

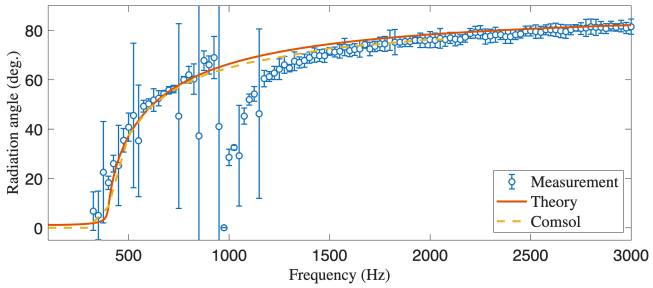


FIG. 12: Radiation angle results from theoretical modeling, finite-element modeling, and measurements, for the antenna with monopole source.

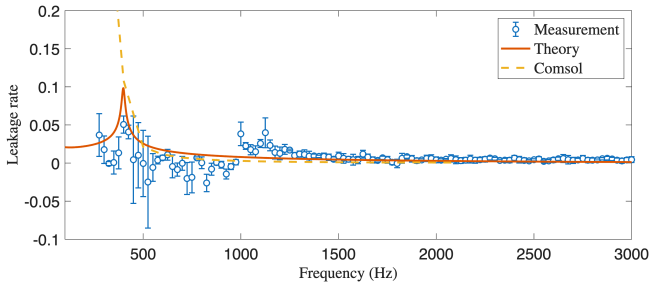


FIG. 13: Resulting leakage factor from theoretical modeling, finite-element modeling, and measurements, for the antenna with monopole source.

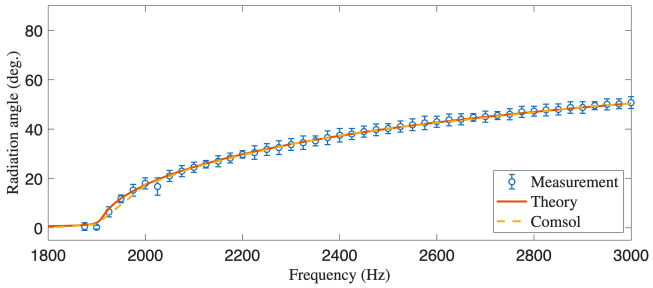


FIG. 14: Radiation angle results from theoretical modeling, finite-element modeling, and measurements, for the antenna with dipole source.

### *2. Measured radiation patterns as function of frequency*

To help further understand the radiation performance of the acoustic leaky-wave antenna, the level response as a function of angle and frequency is plotted in Figs. 16 and 17. The dashed lines in the plots show the radiation angle calculated from the theoretical model.

For the monopole source (Fig. 16), the low-frequency response displays a broad and indistinct directivity up to approximately 1000 Hz, where an unexpected lobe appears at broadside (near 0°) and rapidly increases in angle. Above about 1500 Hz, the response dis-

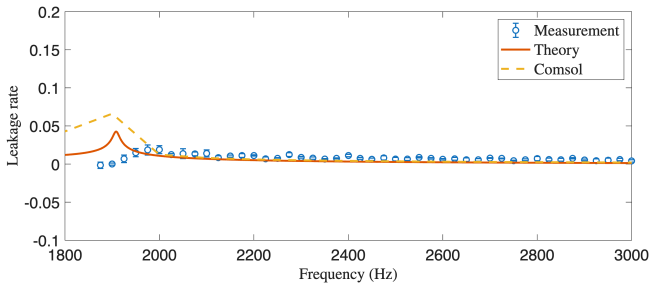


FIG. 15: Resulting leakage factor from theoretical modeling, finite-element modeling, and measurements, for the antenna with dipole source.

plays a less broad, more distinct directivity. These characteristics agree with the discussion above in relation to Fig. 12 and the (0,0) mode. Amplitude variations with peaks separated by about 100 Hz are also observed in the radiation pattern of the (0,0) mode. They are concluded to be attributed to resonances along the length of the antenna, enabled by imperfect termination absorption. At about 1900 Hz, the (1,0) mode begins to emerge, in agreement with the theoretical solution.

For the dipole source (Fig. 17), a distinct directivity is shown from approximately 1900 Hz, in agreement with the theoretical solution for the (1,0) mode. Above about 2000 Hz, sidelobes at angles larger than the main lobe are clearly visible, and less distinct sidelobes can be seen at angles smaller than the main lobe. Moreover, it is interesting to note the increase in response at all angles at about 1900 Hz. An explanation for this may be the increased radiation impedance of the source at the onset of the (1,0) mode.

Figure 18 shows directivity plots of the measured data and of the modeled results of the theoretical solution and numerical calculations for the dipole source at frequencies 2 kHz, 2.5 kHz and 3 kHz. The theoretical directivity patterns were obtained by assuming a longitudinal aperture distribution proportional to $\exp(-(\alpha + j\beta)z)$ over the finite antenna length $L$, and computing the far-field radiation pattern from the spatial Fourier transform of this distribution[24]. The results at the three frequencies show excellent agreement in both the direction and the beamwidth of the main lobe. The results for the first sidelobes can be seen to agree in angle but show some offsets in relative strength. Moreover, angular agreement for the second sidelobes is visible to some extent. The measured data exhibit additional sidelobes that are not seen in the theoretical solution or in the Comsol results; the strongest ones can be concluded to be due to reflection at the termination of the antenna, which is expected to be possible to reduce by using improved absorbers.

The measured results overall support the idea of using the (1,0) mode, with dipole-like excitation, for a frequency-scanning leaky-wave antenna, as it provides good controllability of both the radiation angle and the leakage rate. In addition, the strong agreement between the measured results and the theoretical and numerical predictions of the designed antenna demonstrates a successful validation of the modeling.

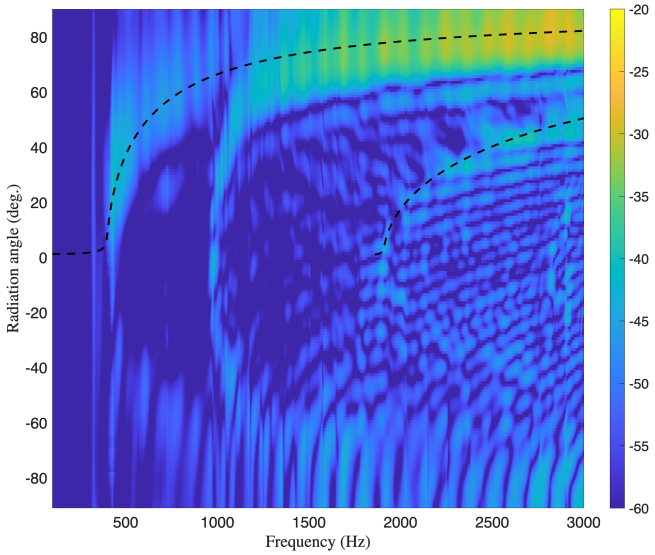


FIG. 16: Directivity plot of the measured data from the antenna with monopole source. Plotted as radiated pressure in dB (re. arb.) as function of angle and frequency. Theoretical radiation angle plotted as dashed lines.

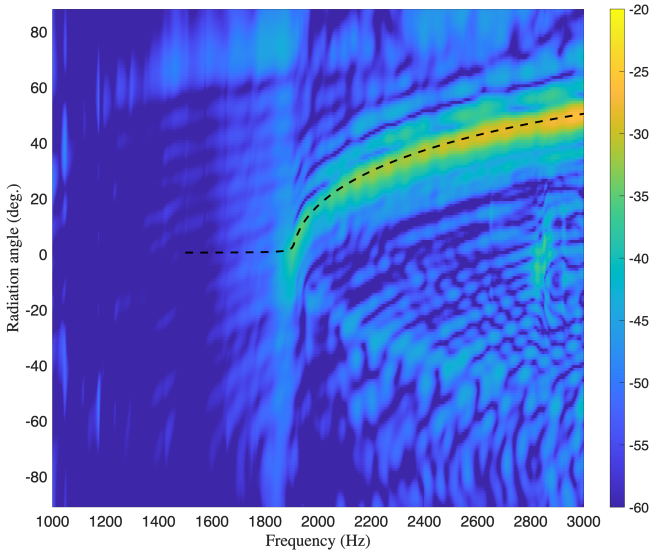


FIG. 17: Directivity plot of the measured data from the antenna with dipole source.

## V. CONCLUSION

The paper presents consistent theoretical modeling, numerical modeling, and measurements of a designed and built acoustic leaky-wave antenna. The results show proof of concept of the acoustic leaky-wave antenna with frequency scanning capability, i.e., that the radiation angle can be controlled by the frequency of the source (the feeding of the antenna).

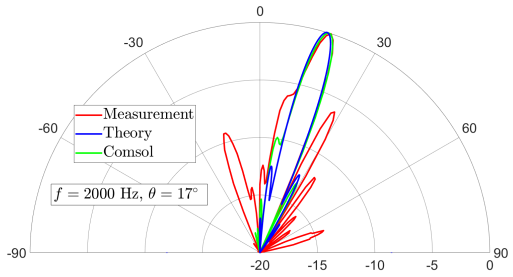


(a) $f = 2000$ Hz.

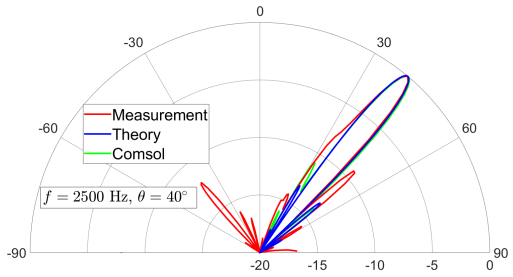


(b) $f = 2500$ Hz.

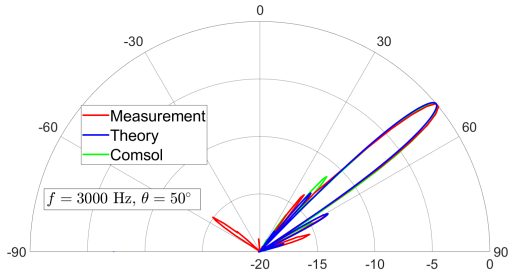


(c) $f = 3000$ Hz.

FIG. 18: Directivity plots from measurements, theoretical modeling, and finite-element modeling for the dipole source at frequencies 2 kHz (a), 2.5 kHz (b), and 3 kHz (c). The directivity is normalized with the maximum value for each frequency and plotted within the range of -20–0 dB.

The presented theory provides the necessary formulations for predicting the two main design parameters, the radiation angle and leakage rate, for uniform or quasi-uniform acoustic leaky-wave antennas. The central parts of the theory include the Transverse Equivalent Network (TEN), the Transverse Resonance Equation (TRE), and the solution of the TRE via the resonance condition on reflection factors, which results in the real and imaginary

parts of the longitudinal wavenumber. For the acoustical setting of hard boundaries, the existence of the (0,0) mode, i.e. a static mode, was identified. Theoretical steps also include a description of the modal solution and of the shapes of the two lowest modes, i.e., mode (0,0) and mode (1,0), as well as the impedance modeling of the perforated wall of the antenna. The developed theoretical model was used for parameter studies of the perforation hole radius and cross-sectional width of the antenna. The results indicated that using the (1,0) mode could be preferable to using the (0,0) mode for frequency scanning due to greater controllability of the radiation angle and leakage rate.

Wave-based modeling is performed using the finite element method, with validity supported by good agreement with the theoretical model in terms of radiation angle and leakage rate for the two modes studied. The validated numerical tool is particularly useful for modeling more complex antenna designs, for example those with non-uniform variations along the antenna length.

Based on the theoretical and numerical results, a prototype antenna was designed and built for use in validating measurements. A source with either monopole or dipole characteristics was used to mainly excite the (0,0) mode or the (1,0) mode, respectively. The measured data showed very good agreement with the modeled results for the radiation angle for the (1,0) mode, while the (0,0) mode showed significant deviations within a range of lower frequencies. The general agreement in leakage rate was good, except for larger deviations below and near peak frequency.

Taken together, the measurement results confirm the validity of the theoretical and numerical modeling, as well as the good frequency-scanning capability of the designed prototype acoustic leaky-wave antenna for the (1,0) mode. For future work, investigations of more complex ALWA designs are of interest, including modulated or tapered geometries, for controlling, e.g., sidelobe levels and beam shape, as well as the incorporation of resonant elements to enable backward-to-forward beam scanning.

## AUTHOR DECLARATIONS

The authors have no conflict to disclose. The data that support the findings of this study are available within the article.

## ACKNOWLEDGMENTS

The work of Astrid Algaba-Brazález is supported by the Grant RYC2022-037385-I funded by MICIU/AEI /10.13039/501100011033 and by ESF+. The work of José Luis Gómez-Tornero, Pablo-Antonio Martínez-Vicente and Astrid Algaba-Brazález is also supported by the Spanish National Project under Grant PID2022-136590OB-C42 funded by MICIU/AEI /10.13039/501100011033 and by FEDER, UE. The research work disclosed in this publica-

tion is partially funded by the ENDEAVOUR II Scholarships Scheme (Malta). Project may be co-funded by the ESF+ 2021-2027.

## REFERENCES

[1]W. W. Hansen, "Radiating electromagnetic wave guide" (1946) US Patent 2,402,622.

[2]D. Jackson and A. Oliner, "Ch. 7: Leaky-wave antennas," Modern Antenna Handbook. Wiley, Hoboken (2008).

[3]D. R. Jackson, C. Caloz, and T. Itoh, "Leaky-wave antennas," Proceedings of the IEEE **100**(7), 2194–2206 (2012).

[4]D. Jackson *et al.*, "The fundamental physics of directive beaming at microwave and optical frequencies and the role of leaky waves," Proceedings of the IEEE **99**(10), 1780–1805 (2011).

[5]C. J. Naify, C.-M. Chang, G. McKnight, and S. Nutt, "Direction finding via acoustic leaky wave antennas," Applied Physics Letters **102**(20), 203508 (2013) doi: 10.1063/1.4807611.

[6]C. J. Naify, "Acoustic leaky wave antennas: Direction finding via dispersion," Ph.D. thesis, California Institute of Technology, Pasadena, CA, USA, 2016, https://resolver.caltech.edu/CaltechTHESIS:06132016-155719912, Ph.D. dissertation.

[7]C. J. Naify, M. Haberman, M. Guild, and C. Sieck, "Acoustic leaky wave antennas: Direction-finding via dispersion," Acoustics Today **14**(3), 31–38 (2018).

[8]Q. Wang, J. Lan, Z. Deng, Y. Lai, and X. Liu, "Acoustic leaky-wave antennas with heterogeneous unit cells for enhanced directivity and localization," The Journal of the Acoustical Society of America **153**(1), 487–495 (2023) doi: 10.1121/10.0016815.

[9]H. Esfahlani, S. Karkar, H. Lissek, and J. R. Mosig, "Acoustic dispersive prism," Scientific reports **6**(1), 18911 (2016).

[10]H. Esfahlani, S. Karkar, H. Lissek, and J. R. Mosig, "Exploiting the leaky-wave properties of transmission-line metamaterials for single-microphone direction finding," The Journal of the Acoustical Society of America **139**(6), 3259–3266 (2016) https://doi.org/10.1121/1.4949544 doi: 10.1121/1.4949544.

[11]I. Felis-Enguix, J. Otero-Vega, M. Campo-Valera, I. Villó-Pérez, and J. L. Gómez-Tornero, "Practical aspects of acoustic leaky-wave antennas applied to underwater direction finding," Engineering Proceedings **2**(1), 93 (2020).

[12]M. Poveda-García, D. Cañete-Rebenaque, and J. L. Gómez-Tornero, "Frequency-scanned monopulse pattern synthesis using leaky-wave antennas for enhanced power-based direction-of-arrival estimation," IEEE Transactions on Antennas and Propagation **67**(11), 7071–7086 (2019).

[13]J. L. Gómez-Tornero, "Smart leaky-wave antennas for iridescent iot wireless networks," Antenna and Array Technologies for Future Wireless Ecosystems 119–181 (2022).

[14]J. A. López-Pastor, M. Poveda-García, A. Gil-Martínez, D. Cañete-Rebenaque, and J. L. Gómez-Tornero, "2-D localization system for mobile IoT devices using a single Wi-Fi access point with a passive frequency-scanned antenna," IEEE Internet of Things Journal **10**(17), 14995–15011 (2023).

[15]T. Fukushima, T. Matsukawa, Y. Ikemura, H. Terasoma, S. Kato, T. Fujihashi, T. Murakami, Y. Asai, and S. Saruwatari, "Wi-Fi meets sound: A deep fusion leap beyond single-modality for device localization," IEEE Access (2025).

[16]C. J. Naify, C. N. Layman, T. P. Martin, M. Nicholas, D. C. Calvo, and G. J. Orris, "Experimental realization of a variable index transmission line metamaterial as an acoustic leaky-wave antenna," Applied Physics Letters **102**(20), 203508 (2013) https://doi.org/10.1063/1.4807280 doi: 10.1063/1.4807280.

[17]J. Lan, X. Peng, X. Zhang, X. Liu, and Y. Li, "Improving directional radiation quality based on a gradient amplitude acoustic leaky wave antenna," New Journal of Physics **21**(10), 103023 (2019).

[18]C. W. Broadman, C. J. Naify, M. J. Lee, and M. R. Haberman, "Design of a one-dimensional underwater acoustic leaky wave antenna using an elastic metamaterial waveguide," Journal of Applied Physics **129**(19), 194902 (2021) https://doi.org/10.1063/5.0044802 doi: 10.1063/5.0044802.

[19]J. Zhang, V. Romero-García, G. Theocharis, O. Richoux, V. Achilleos, and D. J. Frantzeskakis, "High-amplitude sound propagation in acoustic transmission-line metamaterial," Applied Physics Letters **118**(10) (2021).

[20]A. Fernández-Garrido *et al.*, "Parametric study and experimental validation of acoustic leaky wave antenna in spatial localization," IEEE Access **13**, 10371–10385 (2025) doi: 10.1109/ACCESS.2025.3528081.

[21]COMSOL AB, "Comsol multiphysics® acoustics module" , https://www.comsol.com/acoustics-module (2023) version 6.2, Stockholm, Sweden.

[22]T. Zhao, D. R. Jackson, J. T. Williams, and A. A. Oliner, "General formulas for 2-d leaky-wave antennas," IEEE Transactions on Antennas and Propagation **53**(11), 3525–3533 (2005).

[23]J. Hines and J. Upson, "A wide aperture tapered-depth scanning antenna," Ohio State Univ. Res. Found **667**, 10 (1957).

[24]A. A. Oliner, D. R. Jackson, and J. Volakis, "Leaky-wave antennas," Antenna engineering handbook **4**, 12 (2007).

[25]R. Sorrentino and M. Mongiardo, "Transverse resonance techniques," Encyclopedia of RF and Microwave Engineering (2005).

[26]J. L. Gómez-Tornero, J. Pascual-García, and A. Álvarez-Melcón, "A novel full-wave cad for the design of tapered leaky-wave antennas in hybrid waveguide printed-circuit technology," International Journal of RF and Microwave Computer-Aided Engineering **16**(4), 297–308 (2006).

[27]M. Garcia-Vigueras, J. L. Gomez-Tornero, G. Goussetis, A. R. Weily, and Y. J. Guo, "Efficient synthesis of 1-d fabry–perot antennas with low sidelobe levels," IEEE Antennas and Wireless Propagation Letters **11**, 869–872 (2012).

[28]A. J. Martinez-Ros, J. L. Gómez-Tornero, and F. Quesada-Pereira, "Efficient analysis and design of novel siw leaky-wave antenna," IEEE Antennas and Wireless Propagation Letters **12**, 496–499 (2013).

[29]L. E. Kinsler, A. R. Frey, A. B. Coppens, and J. V. Sanders, *Fundamentals of Acoustics (4th Edition)* (John Wiley & Sons, 1999), https://app.knovel.com/hotlink/toc/id:kpFAE00003/fundamentals-acoustics/fundamentals-acoustics.

[30]C. Caloz and T. Itoh, *RadiatedWave Applications*, 261–315 (John Wiley & Sons, Inc.), doi: 10.1002/0471754323.ch6.

[31]M. Poveda-García, A. Algaba-Brazalez, and J. L. Gómez-Tornero, "Rigorous analysis of the different terms contributing to the attenuation constant in uniform leaky-wave antennas, under review," IEEE Transactions on Antennas and Propagation (2025).

[32]M. Poveda-García, A. Algaba-Brazalez, D. Comite, and J. L. Gómez-Tornero, "Impact of the reactive attenuation constant in the efficiency of uniform/quasi-uniform leaky-wave antennas radiating at broadside," in *2025 International Conference on Electromagnetics in Advanced Applications (ICEAA 2025)*, Palermo, Italy (2025).

[33]I. Mann, J. Adin, J. Tichy, and A. J. Romano, "Instantaneous and time-averaged energy transfer in acoustic fields," The Journal of the Acoustical Society of America **82**(1), 17–30 (1987) https://doi.org/10.1121/1.395562 doi: 10.1121/1.395562.

[34]T. E. Vigran, *Building acoustics* (CRC Press, 2008), p. 362.

[35]M. Kleiner, *Electroacoustics* (Taylor & Francis Group, 2013).

[36]R. T. Randeberg, "Perforated panel absorbers with viscous energy dissipation enhanced by orifice design," Ph.D. thesis, Department of Telecommunications, Norwegian University of Science and Technology, 2000.

[37]R. L. Pritchard, "Mutual acoustic impedance between radiators in an infinite rigid plane," The Journal of the Acoustical Society of America **32**(6), 730–737 (1960) https://doi.org/10.1121/1.1908199 doi: 10.1121/1.1908199.

[38]H. Lin, T. Bengisu, and Z. P. Mourelatos, *Lecture Notes on Acoustics and Noise Control* (Springer, 2023).

[39]M. Ysik, "The transcendental property of a guide," Journal of Metaphysical Physics **3**(7) (1981).

[40]The MathWorks, Inc., *fminsearch*, The MathWorks, Inc. (2025), https://www.mathworks.com/help/optim/ug/fminsearch.html, mATLAB R2025a Documentation, Optimization Toolbox.

[41]Comsol, "Perfectly matched boundary" , https://doc.comsol.com/6.0/doc/com.comsol.help.aco/aco_ug_pressure.05.035.html.

[42]Comsol, "External field calculation" , https://doc.comsol.com/5.5/doc/com.comsol.help.aco/aco_ug_pressure.05.024.html.

[43]Comsol, "Sound hard boundary" , https://doc.comsol.com/5.5/doc/com.comsol.help.aco/aco_ug_pressure.05.067.html.

[44]D. I. Havelock, S. Kuwano, and M. Vorländer, *Handbook of signal processing in acoustics*, Vol. 1 (Springer, 2008).

[45]S.-T. Yang and H. Ling, "Two-section half-width microstrip leaky wave antenna," IEEE Transactions on Antennas and Propagation **62**(10), 4988–4996 (2014) doi: 10.1109/TAP.2014.2345578.